River plume patterns and dynamics within the Southern California Bight

J.A. Warrick[a,*], P.M. DiGiacomo[b], S.B. Weisberg[c], N.P. Nezlin[c], M. Mengel[d],
B.H. Jones[e], J.C. Ohlmann[f], L. Washburn[f], E.J. Terrill[g], K.L. Farnsworth[a]

[a]*USGS Coastal and Marine Geology Program, Santa Cruz, CA 95060, USA*
[b]*NOAA/NESDIS Center for Satellite Applications and Research (STAR), Camp Springs, MD 20746, USA*
[c]*Southern California Coastal Water Research Project (SCCWRP), Costa Mesa, CA 92626, USA*
[d]*Orange County Sanitation District (OCSD), Fountain Valley, CA 92728, USA*
[e]*Department of Biological Sciences, University of Southern California, Los Angeles, CA 90089, USA*
[f]*Institute for Computational Earth System Science (ICESS), University of California, Santa Barbara, Santa Barbara , CA 93106, USA*
[g]*Marine Physical Laboratory, Scripps Institute of Oceanography, La Jolla, CA 92093, USA*

Abstract

Stormwater river plumes are important vectors of marine contaminants and pathogens in the Southern California Bight. Here we report the results of a multi-institution investigation of the river plumes across eight major river systems of southern California. We use *in situ* water samples from multi-day cruises in combination with MODIS satellite remote sensing, buoy meteorological observations, drifters, and HF radar current measurements to evaluate the dispersal patterns and dynamics of the freshwater plumes. River discharge was exceptionally episodic, and the majority of storm discharge occurred in a few hours. The combined plume observing techniques revealed that plumes commonly detach from the coast and turn to the left, which is the opposite direction of Coriolis influence. Although initial offshore velocity of the buoyant plumes was ~50 cm/s and was influenced by river discharge inertia (i.e., the direct momentum of the river flux) and buoyancy, subsequent advection of the plumes was largely observed in an alongshore direction and dominated by local winds. Due to the multiple day upwelling wind conditions that commonly follow discharge events, plumes were observed to flow from their respective river mouths to down-coast waters at rates of 20–40 km/d. Lastly, we note that suspended-sediment concentration and beam-attenuation were poorly correlated with plume salinity across and within the sampled plumes (mean $r^2 = 0.12$ and 0.25, respectively), while colored dissolved organic matter (CDOM) fluorescence was well correlated (mean $r^2 = 0.56$), suggesting that CDOM may serve as a good tracer of the discharged freshwater in subsequent remote sensing and monitoring efforts of plumes.
Published by Elsevier Ltd.

1. Introduction

Southern California's coastal watersheds (Fig. 1a) drain a highly modified landscape with 54% of the

*Corresponding author. Tel.: + 1 831 427 4793.
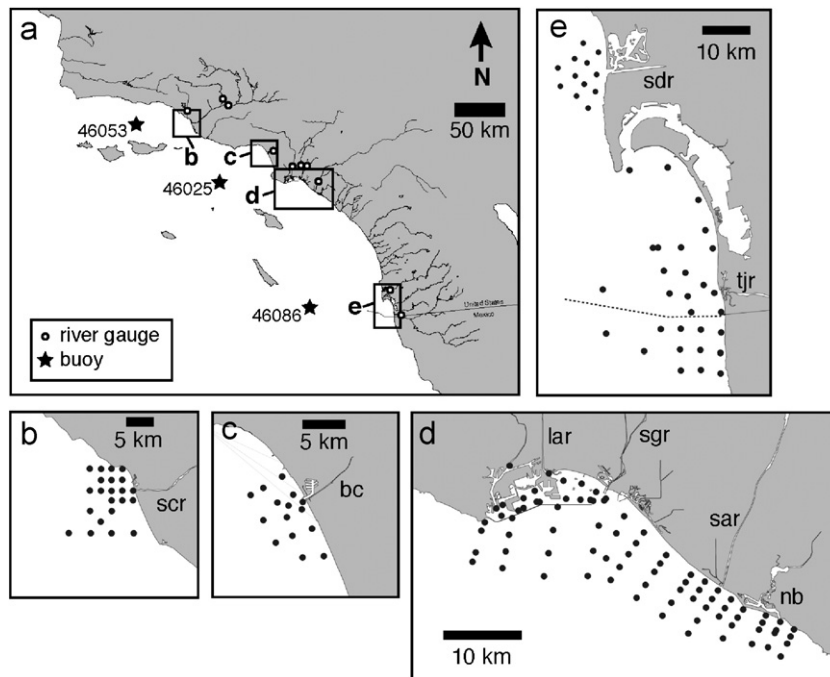E-mail address:* jwarrick@usgs.gov (J.A. Warrick).

Fig. 1. (a) The Southern California Bight study area with the four sampled regions identified. (b)–(e) Ship-based plume sampling stations for each of the four regions. Rivers are also identified: scr—Santa Clara River, bc—Ballona Creek, lar—Los Angeles River, sgr—San Gabriel River, sar—Santa Ana River, nb—Newport Bay, sdr—San Diego River and tjr—Tijuana River.

watershed area dammed and many of the channels straightened, leveed or channelized (Willis and Griggs, 2003). These modifications, combined with the Mediterranean climate, lead to episodic river discharge, with large winter storms contributing the majority of annual water and sediment budgets (Inman and Jenkins, 1999). These river systems also provide large loadings of pollutants and pathogens to the coastal ocean, surpassing loadings from municipal wastewater discharges for most constituents and as such merit detailed investigation (Schiff et al., 2001; Dojiri et al., 2003; Warrick et al., 2005; Ahn et al., 2005; Stein et al 2006).

The plumes from these river discharge events can extend 10's of km from the shoreline (Mertes and Warrick, 2001; DiGiacomo et al., 2004; Nezlin and DiGiacomo, 2005; Nezlin et al., 2005). Nezlin et al. (2005) found that plume areas defined by SeaWiFS radiometer-data were strongly correlated to antecedent precipitation. The maximum extent of these plumes occurs 1–3 days following precipitation, and multiple day plume persistence was found for all of the major river plumes (Nezlin et al., 2005). However, significant plume size variability is found across the California watersheds in both time and space (Mertes and Warrick, 2001; Warrick and

Fong, 2004; Nezlin and DiGiacomo, 2005; Nezlin et al., 2005).

Jones and Washburn (1997), Washburn et al. (2003) and Warrick et al. (2004a) have shown that the freshwater from southern California rivers quickly stratifies into a buoyant plume when it reaches the ocean. Warrick et al. (2004b) suggest that the movement of Santa Clara River plume near the river mouth is strongly influenced by the river discharge inertia, i.e., the momentum induced by the mass flux from the river. These river plumes are also likely subject to buoyancy, wind and tidal forcing, which will dictate dispersal patterns and dynamics (e.g., Stumpf et al., 1993; Garvine, 1995; Piñones et al., 2005; Whitney and Garvine, 2005). Better understanding of plumes in the Southern California Bight is needed to track and understand the potential health and ecological implications of the discharged pollutants.

Finally, satellite-derived ocean color products have been valuable tools to investigate the lateral movement of southern California river plumes, and most of these investigations utilize turbidity or suspended-sediment products as proxies to track plumes (e.g., Mertes and Warrick, 2001; Nezlin et al., 2005). Although these river plumes are

commonly quite turbid, sediment mass balances suggest that little of the discharged sediment resides in the buoyant plume due to rapid settling near the river mouth (Warrick et al., 2004a). It is necessary and valuable, then, to evaluate which satellite-based measurements may best track the freshwater plumes.

Here we present the results of a multi-organiza- tion study to describe post-storm runoff plumes from the eight largest river systems in southern California. Each of these systems was assessed for up to 5 days following each of two storms during 2004 and 2005. We combine *in situ* and remotely sensed data to evaluate plume dispersal patterns and rates and the forcing function(s) responsible for these transformations. Emphasis is placed on identifying transport and transformations processes that could be generalized across systems and discharge events.

2. Methods

The study involved sampling four geographic regions that represent the river mouths of the largest southern California watersheds (Fig. 1). These regions included (from the north): the eastern Santa Barbara Channel (Santa Clara and Ventura Rivers); Santa Monica Bay (Ballona Creek); the San Pedro Shelf (Los Angeles, San Gabriel and Santa Ana Rivers); and the southern Bight (San Diego and Tijuana Rivers). These regions and river systems were chosen because they represented a broad distribution of watershed land use and river types (open space, agricultural and urban) and because they covered the broad geographic extent of southern California.

Here, we provide a summary of the methods used to investigate the river plumes; details of the data collection methods, quality assurance/quality con- trol program, and raw data will be published in the Bight'03 Water Quality Study Final Report (Southern California Water Research Project (SCCWRP), in preparation). The primary method of investigation was shipboard profiling of the plumes with an enhanced CTD system (conductivity, temperature, depth, dissolved oxygen, pH, transmissometer, chlorophyll fluorometer, and CDOM fluorometer), hereafter referred to as CTD + . Water turbidity was computed from transmissometer observations as the beam attenuation coefficient at 660 nm (hereafter referred to as beam-c). CDOM fluorescence was linearly calibrated with up to 100 ppb of quinine

sulfate dehydrate (QSD). Water samples were obtained with 5-l Niskin bottles attached to the CTD + carrousel and triggered remotely. Sampling occurred on regularly spaced grids for each region, which are shown in Fig. 1. The primary intent of the grids was to sample the nearshore discharge areas and assess water quality there, not necessarily to track plumes as they advected away from the river mouth regions. Some stations were positioned further offshore so that they provided ''non-plume'' profiles for comparative purposes. Profiles were obtained to within 2 m of the seabed or to a depth of 60 m for sites deeper than 60 m. Water samples were taken at 1 m water depth for most sites and at a sub- surface depth(s) below the buoyant plume for a limited number of sites. Samples were analyzed for total suspended solids, chlorophyll, macronutrients (Si, N, P), bacteria and toxicity. Here we focus primarily on the measurements of salinity, tempera- ture and suspended solids; the remaining data will be presented in subsequent publications.

The sampling plan called for sampling two events across each region, and 3 days of sampling during each event as conditions permitted (to be nominally conducted on days 1, 3 and 5 following the discharge peak). One ship was dedicated to each region, except for the San Pedro Shelf where three monitoring vessels were utilized coincidentally and the Tijuana River where two ships were used. However, not all sites were sampled in the proposed fashion largely due to limitations from weather and sea-state (Figs. 2 and 3). Further, sampling of the Tijuana River plume was conducted during an event not sampled at the remaining sites (Fig. 3), due to a storm that was directed largely toward the southern portion of the study area. The resulting sampling effort consisted of 574 CTD + stations and 705 water samples during a total of 36 ship-days.

Ancillary data were also collected or utilized to supplement the shipboard sampling. River dis- charge observations were obtained from US Geo- logical Survey (USGS) gauging stations, stations operated by Los Angeles County Department of Public Works (LACDPW), and a daily discharge gauge for the Tijuana River operated by the International Boundary and Water Commission (Fig. 1). USGS sites provided discharge rates at 15-min intervals and included the following sites: Ventura River (USGS station 11118500), Santa Clara River (sum of USGS 11113000 and 11109000), Santa Ana River (USGS 11078000), and the San Diego River (USGS 11023000).
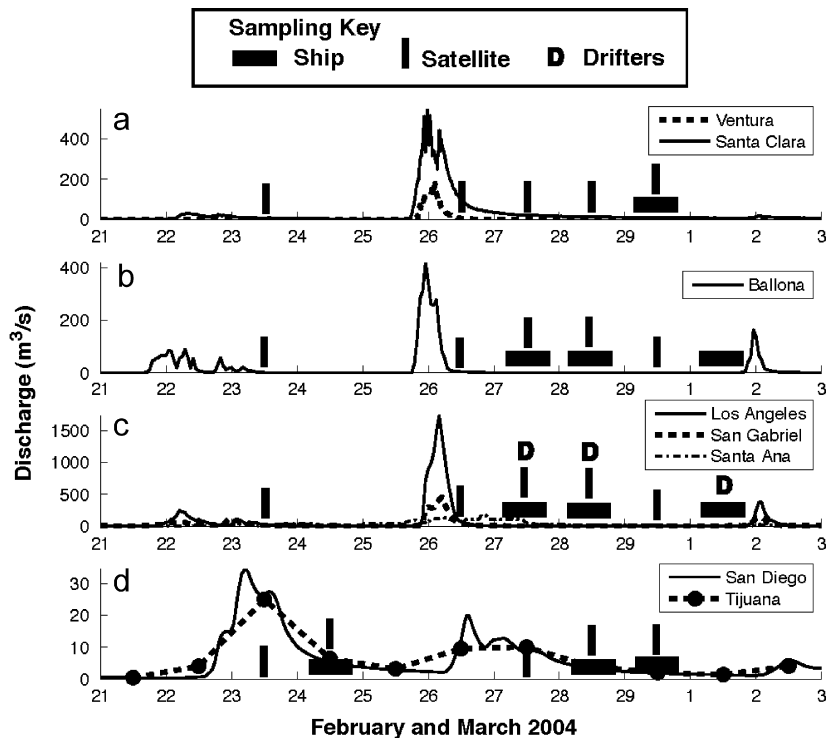
Fig. 2. Discharge and sample timing for the first event sampled.

LACDPW stations provided discharge rates at 1-h intervals and included Ballona Creek (station F38C), Los Angeles River (F319), and San Gabriel River (sum of F354 and F42B).

Hourly averaged wind speed and direction were obtained from a number of the NDBC buoys, including 46053 (East Santa Barbara Channel), 46025 (Santa Monica Basin) and 46086 (San Clemente Basin; Fig. 1). These data were used to evaluate the influence of wind speed and wind stress on the river plumes, where wind stress (τ_w) was computed by the iterative quadratic formulation of Large and Pond (1981) for each hourly measurement.

Satellite ocean color imagery was obtained from the NASA Moderate Resolution Imaging Spectro-radiometers (MODIS) on the Aqua and Terra platforms. These sensors provided daily or better coverage of the Southern California Bight study area, although clear-sky images were obtained for only about half of the days of interest and largely on days following river discharge peaks (Figs. 2 and 3). Here we present "true-color" representations of the multi-band data provided by each sensor to qualitatively track the combined sediment, CDOM and phytoplankton manifestations of the buoyant plume. Quantitative satellite-derived products (e.g., a412, bb551, chlorophyll-*a*) are discussed in a companion paper to better understand the impacts of the plumes (Nezlin et al., in preparation).

Surface currents were obtained from the tracks of high-resolution drifting buoys drogued at 1 m depth (Ohlmann et al., 2005). The drifters, with known water following capabilities, record their position every 10 min using GPS. Individual drifter tracks give an indication of how river plume water moves in the coastal ocean. The relative motion of drifter pairs allows for quantification of plume dispersion. Sets of up to 21 drifters were released within the river plumes just beyond the surf zone at the Santa Clara River (1 day), Santa Ana River (6 days) and the Tijuana River (3 days). The drifters were typically released in the morning and retrieved before sunset. If a drifter was clearly about to enter the surf zone, thus being subject to damage, it was retrieved and re-deployed offshore of the river mouth. The individual drifter tracks along with flow information determined from the position data can be viewed on the web at (www.drifterdata.com).

Lastly, high-frequency (HF) radar was used for the Santa Clara/Ventura and Tijuana River systems to track surface currents during the sampled events.
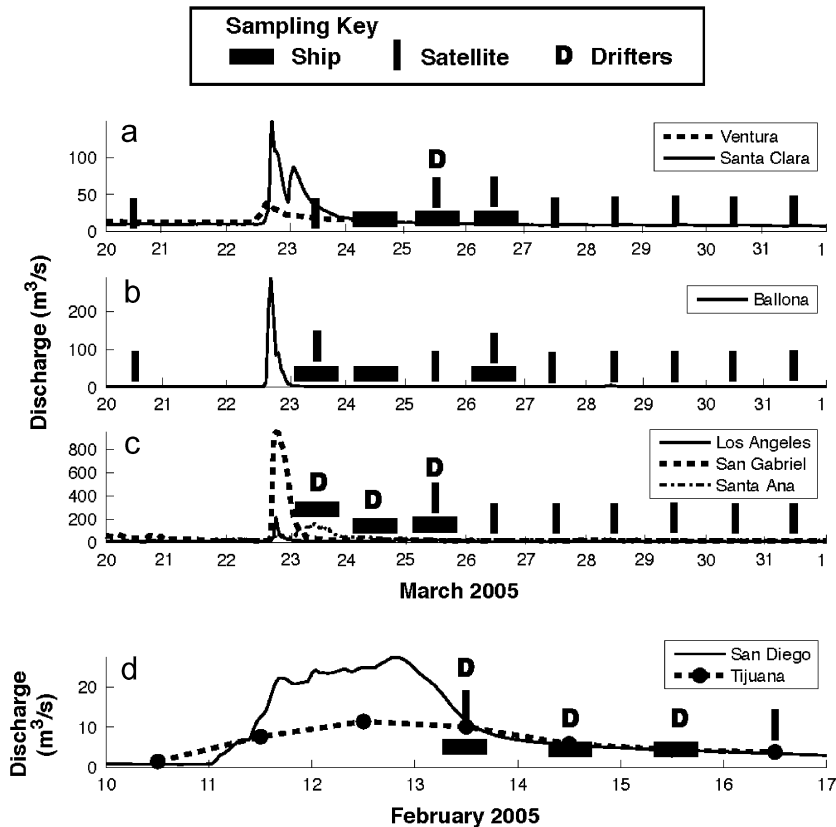
Fig. 3. Discharge and sample timing for the second event sampled. Note that the Tijuana River (d) was sampled on a different schedule than the other systems (a–c).

The northern HF radar array is part of the UCSB Ocean Surface Currents Mapping Project, which consists of 4 sites to characterize surface currents in the Santa Barbara Channel (http://www.icess.ucsb.edu/iog/realtime/index.php). The Tijuana River region is included in the San Diego Coastal Ocean Observing System (SDCOOS) administered by Scripps Institution of Oceanography (SIO; http://sdcoos.ucsd.edu/).

3. Results

3.1. General plume patterns

Two events were sampled for each river mouth region during the winters of 2004 and 2005 (Figs. 2 and 3). The 2004 event resulted in approximately twice the discharge rates and volumes of the 2005 events. Both events were modest sized, however, as the peak discharges were equivalent to approximately 2- and 1.5-year recurrence interval events based on longer discharge records. Therefore, the

sampled events were slightly smaller than the "annual" recurrence events (i.e., the 2.3-year recurrence event) for each river.

Ship-based sampling occurred within 1–5 days of the discharge events (Figs. 2 and 3). However, the 2004 event was generally more difficult to sample due to sea-state. Sampling for the Santa Clara River during 2004 was only possible on the fourth day following peak discharge (Fig. 2a). Sampling of Ballona Creek was very limited on February 27, 2004 due to sea-state and only 4 stations were sampled. The 2005 efforts resulted in sampling immediately following discharge and for 3 full days of sampling for each region (Fig. 3).

Two representative profiles of salinity and beam-c from the Tijuana River plume are shown in Fig. 4. Both profiles were obtained approximately 4-km from the river mouth on February 14, 2005, and both show a freshened buoyant plume in the upper 3–5 m of the water column. Similar plume observations were obtained throughout the other study areas. These buoyant surface plumes also had
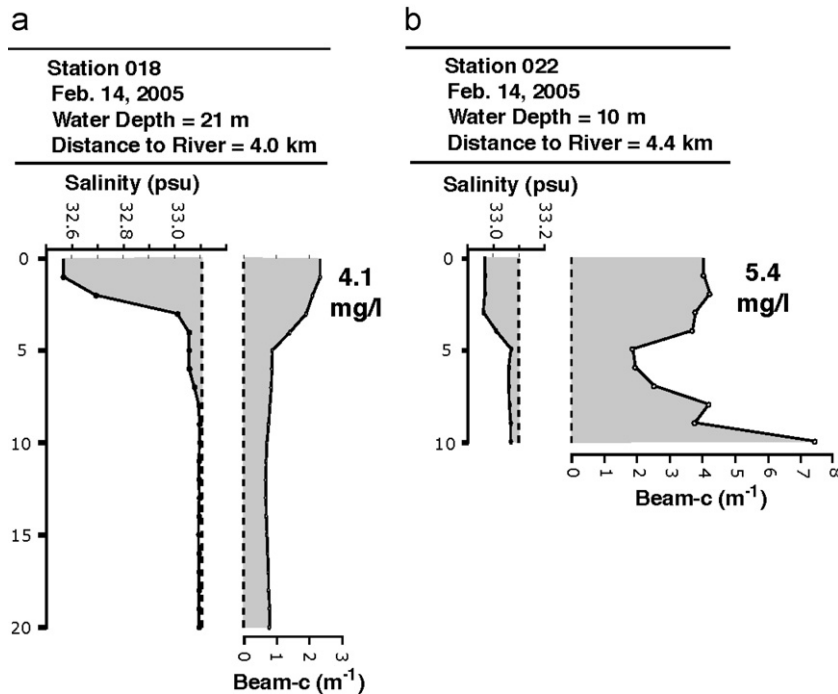
Fig. 4. Example salinity, beam-c and TSS data from CTD casts taken on February 14, 2005 offshore of the Tijuana River. TSS concentrations are shown for 1 m water depth samples. Dashed lines represent reference levels of 33.1 psu salinity and $0 \, m^{-1}$ beam-c.
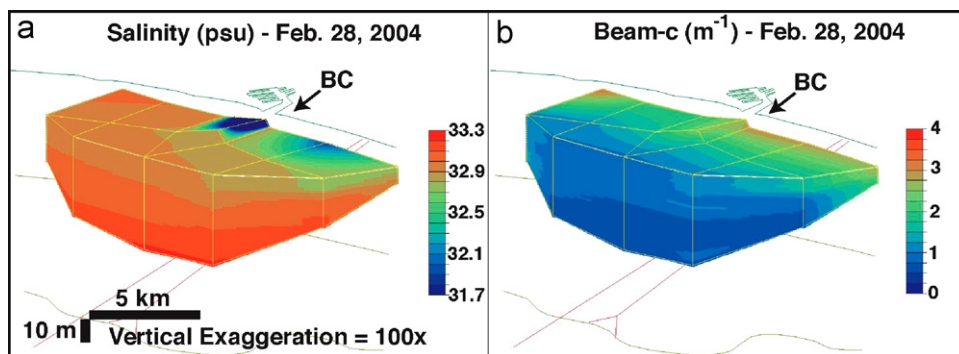

Fig. 5. Three-dimensional presentation of salinity and beam-c data offshore of Ballona Creek (BC) showing the freshened and turbid river plume waters along the sea-surface. Linear interpolation has been used to estimate parameter values between stations, which are shown with vertical yellow lines and line intersections along the water surface.

elevated beam-c compared to waters immediately underneath the plume (Fig. 4). The waters immediately above the seabed differ considerably, however: the shallower station (Fig. 4b) reveals an ~5 m nephloid layer above the seabed, which was a common characteristic of many of the shallow profiles, while the deeper profile did not (Fig. 4a). It is instructive, however, to also contrast the buoyant plumes: the deeper station (Fig. 4a) had lower salinity (i.e., more freshwater) while having

lower suspended sediment (i.e., beam-c and TSS) than the shallow station (Fig. 4b). This suggests that the river water and sediment were not mixing in a simple conservative manner with respect to a single river endmember water type. Below we show that this one observation from the Tijuana River plume was typical of a generally poor relationship between salinity and sediment concentration in stormwater plumes over the entire Southern California Bight.

Spatial mapping of the salinity and beam-c data from each site revealed synoptic characteristics of the buoyant plume properties. For example, data from Ballona Creek on February 28, 2004 show a buoyant plume with lowest salinities immediately offshore of the river mouth, and these low salinities continue to the southern side of the river mouth, which is in the opposite direction of Coriolis influence (Fig. 5a). In contrast, the highest beam-c on the same day was measured close to shore and away from the river mouth (Fig. 5b). The three-ship monitoring effort along the San Pedro Shelf on March 25, 2005 revealed that low salinity/high beam-c waters extended many kilometers along- and across-shore from the river mouths (Fig. 6). Further, it appears that a portion of this broad plume was detached from the coastline, because two regions of low salinity and high turbidity on this date were observed ∼5 km offshore of the coast and laterally offset from the river mouths (Fig. 6).

These two synoptic examples of plume salinity and turbidity (Figs. 5 and 6) reveal another pattern

consistent with all of the remaining sampling dates: although the sampling grids extended many kilometers along- and across-shore, low salinity plumes always extended beyond the geographical limits of the surveys. Thus, none of the surveys captured the "entire" extent of the river plume, as was anticipated.

3.2. Plume freshwater volume calculations

The volume of freshwater residing in the plumes each day can be estimated by spatially integrating the reduced salinity measurements across the sampling grid (cf. Gilbert et al., 1996). For each profile a freshwater fraction (F_{fw}, in m of freshwater) was calculated by

$$F_{fw} = \int_z \{[S_0 - S(z)]/S_0\}\, dz, \tag{1}$$

where S_0 is a reference salinity (in psu), S is the measured salinity (in psu) at depth z (in m). We selected S_0 from the profiles outside of the influence of the plumes either laterally or from the waters underlying the plumes. Unique values of S_0 were calculated for each event within each of the four regions, however similar values of 33.0 psu during 2004 and 33.1 psu during 2005 were obtained for all of the sites. Uncertainty in these values of S_0 was approximately 0.1 psu, which induced less than 10% error across the freshwater volumetric calculations. To compute freshwater volumes we assumed that F_{fw} changed linearly between each station. Further, if $S(z)$ was greater than S_0 for any depth, we set the quantity $[S_0 - S(z)]$ equal to zero.

Results of the volumetric calculations reveal that 10's of millions of cubic meters of freshwater could be accounted for within the survey limits (Tables 1 and 2). The greatest amounts of freshwater were consistently observed along the San Pedro Shelf portion of the study, which not only had the largest river discharge inputs (Figs. 2 and 3) but also had a sampling area 2–20 times larger than the other sites (Tables 1 and 2). The volume of freshwater observed within the survey areas generally decreased with sample date, which suggests that plume waters moved outside of the sampling grids, rather than simply mixing down into the water column.

A couple of exceptions to this multiple-day pattern exist, and they can largely be accounted for by changes in the sampling grids. For example, only a limited sampling effort was possible on the San Pedro Shelf on March 24, 2005 (31.4 km² versus
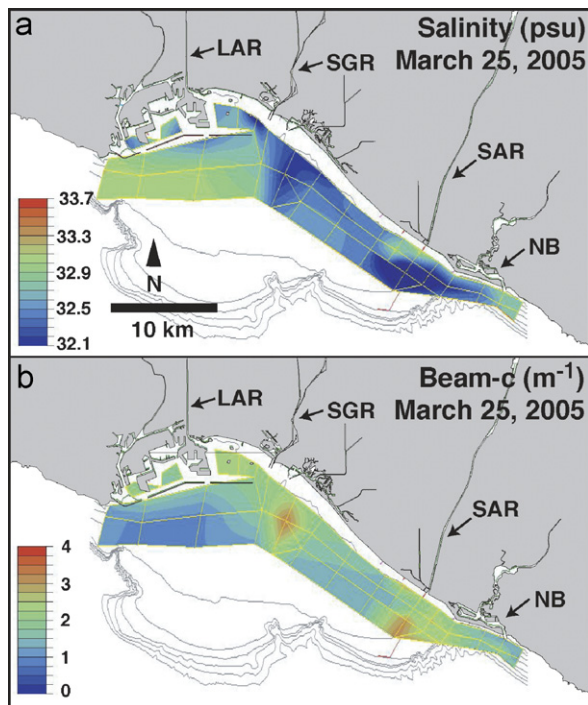

Fig. 6. Surface measurements of salinity and beam-c data from the San Pedro Bay on March 25, 2005. Linear interpolation has been used to estimate parameter values between stations, which are located at the intersections of the yellow lines. The three main river mouths and a bay are also identified (LAR—Los Angeles River, SGR—San Gabriel River, SAR—Santa Ana River, NB—Newport Bay).

Table 1
Integrated CTD survey results for the 2004 surveys

	Santa Clara River	Ballona Creek	San Pedro Shelf	San Diego River	Tijuana River
Area surveyed (km^2)					
24-Feb-2004	–	–	–	10.2	35.9
27-Feb-2004	–	[a]	155.9	–	–
28-Feb-2004	–	35.2	291.0	–	114.5
29-Feb-2004	76.8	–	–	–	114.5
1-Mar-2004	–	35.2	291.0	–	–
Integrated fresh water (m^3)					
24-Feb-2004	–	–	–	79,501	1,362,000
27-Feb-2004	–	[a]	27,512,000	–	–
28-Feb-2004	–	1,264,700	21,003,000	–	411,680
29-Feb-2004	34,570	–	–	–	88,899
1-Mar-2004	–	321,870	16,503,000	–	–
Surface plume sediment mass (t)					
24-Feb-2004	–	–	–	42	1577
27-Feb-2004	–	[a]	31,709	–	–
28-Feb-2004	–	1027	4744	–	1076
29-Feb-2004	1740	–	–	–	1171
1-Mar-2004	–	864	2114	–	–
Ratio of fresh water to sediment (kg/m^3)					
24-Feb-2004	–	–	–	0.53	1.16
27-Feb-2004	–	[a]	1.15	–	–
28-Feb-2004	–	0.81	0.23	–	2.61
29-Feb-2004	50.33	–	–	–	13.17
1-Mar-2004	–	2.68	0.13	–	–

[a]Data collection not adequate to spatially integrate.

the typical ~230 km^2), which resulted in much less freshwater observed (Table 2). The 2005 data from the Tijuana River plume suggested that freshwater volume in the plume doubled on the last day of sampling (Table 2), however the sampling grid was significantly altered on this date in an attempt to capture the presumably northward transporting plume. This modified sampling plan also resulted in capturing another reduced salinity plume from Mission Bay. Lastly, sampling of the Santa Clara River suggested increases in the freshwater plume volume with time (Table 2). Although this is correct, we note below that the portion of the river discharge flux actually observed in this plume was insignificant on all days.

The ratios between the observed plume freshwater volume and the river discharge volume were computed and are shown in Fig. 7. We included an additional amount of river discharge for the third day of the 2005 Tijuana River observations equal to the San Diego River discharge because the ungauged watershed area discharging into San Diego Bay is approximately equivalent to the watershed area of the San Diego River.

A substantial portion of the river discharge volume was observed during most cruise dates, although these values typically decrease with sample date (Fig. 7). Significant variability also exists across the study regions. As alluded to above, there was consistently negligible river water observed offshore of the Santa Clara River mouth (Fig. 7). We suggest below that this river water was transported to the south of the sampling grid due to wind-dominated alongshore currents as discussed below. For Ballona Creek, San Pedro Shelf and Tijuana River, between 35% and 65% of the river water could be accounted for during the first day following a peak discharge date (Fig. 7). Although these ratios appear relatively high compared to the remaining observations, they also suggest that roughly half of the river water had advected away from the sampling grids in the first day of plume formation. The rate of removal of freshwater from the sampling grids on subsequent days ranged 12% of the remaining water per day (San Pedro Shelf) to 80% per day (Tijuana River) for these three sites (mean ± std. dev. = 37 ± 23% per day).

Table 2
Integrated CTD survey results for the 2005 surveys

	Santa Clara River	Ballona Creek	San Pedro Shelf	Tijuana River
Area surveyed (km²)				
13-Feb-2005	–	–	–	81.0
14-Feb-2005	–	–	–	81.0
15-Feb-2005	–	–	–	83.1
23-Mar-2005	–	–	226.5	–
24-Mar-2005	28.9	35.2	31.4	–
25-Mar-2005	28.9	–	228.5	–
26-Mar-2005	28.9	35.2	–	–
Integrated fresh water (m³)				
13-Feb-2005	–	–	–	1,918,000
14-Feb-2005	–	–	–	1,645,400
15-Feb-2005	–	–	–	3,536,000
23-Mar-2005	–	–	23,270,000	–
24-Mar-2005	21,800	2,805,000	1,322,000	–
25-Mar-2005	35,190	–	11,754,000	–
26-Mar-2005	51,440	1,661,000	–	–
Surface plume sediment mass (t)				
13-Feb-2005	–	–	–	960
14-Feb-2005	–	–	–	602
15-Feb-2005	–	–	–	1539
23-Mar-2005	–	–	5894	–
24-Mar-2005	4133	273	575	–
25-Mar-2005	1014	–	2207	–
26-Mar-2005	939	60	–	–
Ratio of fresh water to sediment (kg/m³)				
13-Feb-2005	–	–	–	0.50
14-Feb-2005	–	–	–	0.37
15-Feb-2005	–	–	–	0.44
23-Mar-2005	–	–	0.25	–
24-Mar-2005	189.59	0.10	0.43	–
25-Mar-2005	28.82	–	0.19	–
26-Mar-2005	18.25	0.04	–	–

3.3. Plume sediment and CDOM relationships

As noted above, patterns of salinity and sediment generally did not correlate well. A compilation of all total suspended solids (TSS) and salinity samples shows that salinity explained very little of the variance in the TSS data across the region during the surveys ($r^2 = 0.02$; data not shown). In fact, the three highest measured concentrations of TSS (45–80 mg/l) occurred in waters with negligible freshwater. Salinity and beam-c also correlated poorly, and very little of the beam-c variance could be explained by salinity ($r^2 = 0.15$; data not shown). These poor relationships did not exist only for the data when considered in bulk, but also existed when individual sample days were considered for each river system (Fig. 8). Although one sample date had excellent salinity–TSS correlation ($r^2 = 0.94$; Fig. 8),

we note that this was for the Santa Clara River during the 2004 sample date when little of the river water was observed (cf. Fig. 7).

The fluorometer CDOM concentrations correlated much better with salinity than did either TSS or beam-c (overall $r^2 = 0.58$; mean of individual $r^2 = 0.56$; Fig. 8). No significant ($p < 0.05$) relationships between sample date and CDOM correlation coefficients were found, although slight decreases in linear regression slope with sample date was observed in most data. The CDOM correlations were consistently poor for the Santa Clara River data ($r^2 = 0.32 \pm 0.14$), and this may be due to either the limited river water observed or actual variability in the river water characteristics. Much better CDOM correlations existed for Ballona Creek ($r^2 = 0.65 \pm 0.28$) and the San Pedro Shelf ($r^2 = 0.54 \pm 0.28$), while CDOM fluorescence was not measured for the Tijuana River system. We discuss the implications of these observations to remote sensing of these river plumes in the Discussion section below.

Although the relations between salinity and sediment concentrations were poor, the TSS and beam-c data were adequate to estimate the mass of sediment in the buoyant river plumes. To estimate sediment mass we used a similar spatial integration method as used in the freshwater volume calculations above. For each CTD+ station we computed the plume sediment mass (*Sed*, in g/m²) by

$$Sed = \int_z a[C_p(z) - C_O]\,dz, \qquad (2)$$

where C_p is the measured beam-c profile (in m^{-1}) with respect to depth (z, in m) within the buoyant plume, C_O is the ambient ocean water beam-c defined from our data to be $1\,\mathrm{m}^{-1}$ (cf. Figs. 4–6), and α is a coefficient (in mg-m/l) converting beam-c to suspended-sediment concentration. As noted, calculations were limited to the surface buoyant plume by limiting the *Sed* calculations to portions of the profiles with salinities less than the plume thresholds discussed above (33.0 and 33.1 psu). Further, if $C_p(z)$ was less than C_O we set $[C_p(z) - C_O]$ equal to zero.

To calculate α we compared the TSS and beam-c data from the surface water samples. A significant linear relationship forced through the origin was found between these variables, and beam-c explained almost half the variability in TSS. This relationship was much better during 2004 than 2005 (r^2 of 0.61 and 0.39, respectively), although the
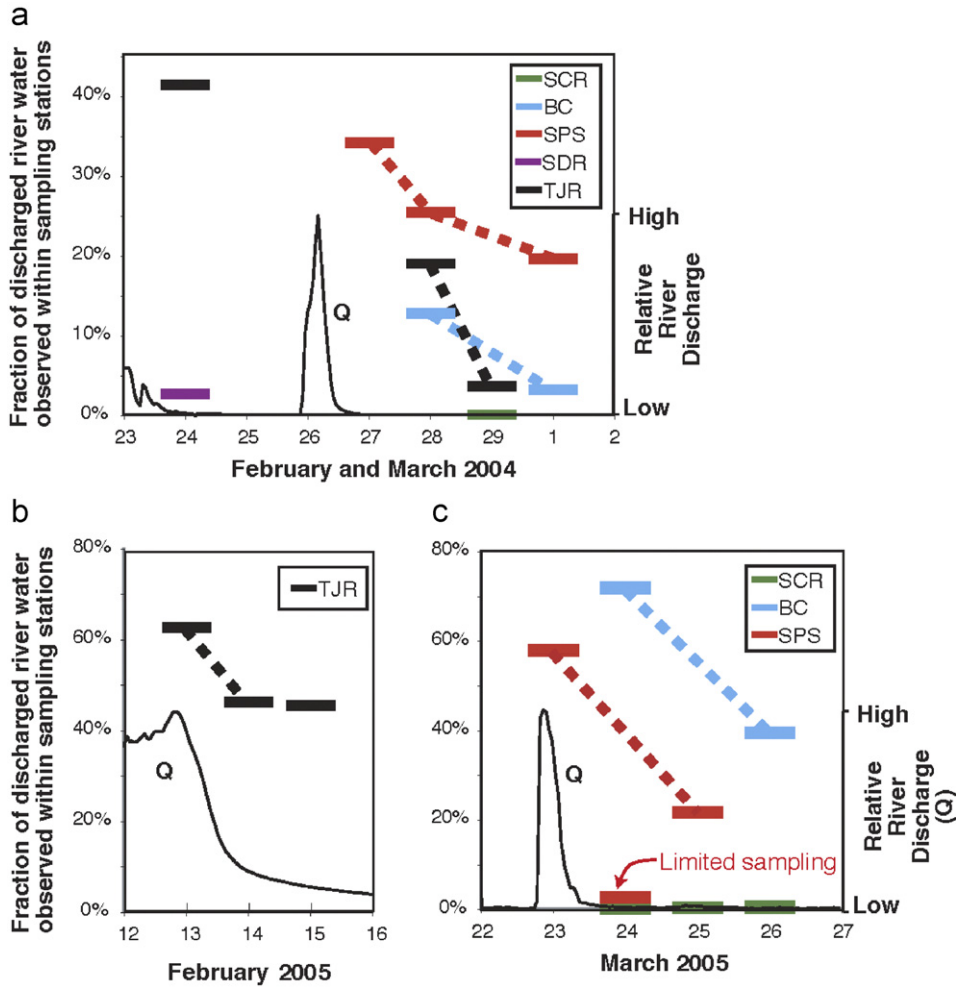
Fig. 7. Integrated plume fresh water observed during the surveys as a proportion of the total event river discharge. Sites include Santa Clara River (SCR), Ballona Creek (BC), San Pedro Shelf (SPS), San Diego River (SDR), Tijuana River (TJR). A discharge (Q) curve is also presented based upon the mean discharge shown in Figs. 2 and 3. Note the differences in scale between (a), (b) and (c).
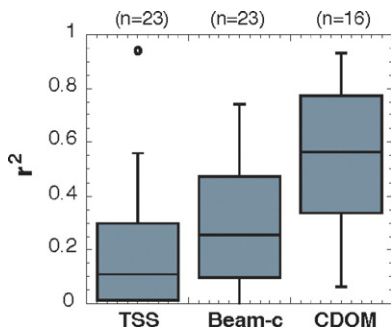

Fig. 8. Box-plots of the correlation coefficients from site-specific linear regressions of TSS, beam-c and CDOM with salinity during each sampling date. Total number of regressions (n) differ because the Tijuana River plume was not sampled for CDOM. Boxes are defined by quartiles, lines show the limits of the data within 1.5 times the interquartile distance from the quartiles, and outliers are shown with circles.

slopes during these two periods were not significantly different ($p < 0.05$). The correlation differences between TSS and beam-c may be a result of: (1) differences in sampling technique—bottle samples versus *in situ* optical samples, and/or (2) grain-size variability in the sediment, which is known to induce significant variability in α (Baker and Lavelle, 1984). Although it is difficult to assess the causes of the variability in the data, we note that the value of α derived from this data (1.65 mg-m/l) is both near the suggested value of 1.4 mg-m/l for clay and fine silt particles by Baker and Lavelle (1984) and consistent with data from the Santa Clara River plume reported by Warrick et al. (2004a). Lastly, we note that relationship between F_{fw} and *Sed* was also very poor ($r^2 = 0.01$; data not shown), which is consistent with other results discussed above.

The calculated mass of sediment contained within the buoyant plumes ranged from O(10) to O(10,000) t on the various sampled dates, and sediment mass within each sampled plume generally decreased with sampling date (Tables 1 and 2). The river suspended-sediment concentration, if sediment mixed conservatively, was estimated by the ratio of observed plume sediment to plume fresh water (Tables 1 and 2). This sediment:water ratio was 0.1–1.2 kg/m^3 for first day of sampling from all the systems but the Santa Clara (the Santa Clara had very little water sampled and first day ratios in excess of 50 kg/m^3). We note that actual river suspended-sediment concentrations during these events were likely ~10 times higher than these ratios (Brownlie and Taylor, 1981; Warrick and Milliman, 2003). Further, although thousands of tonnes of sediment were estimated in the plumes (Tables 1 and 2), these amounts were consistent to other measurements of southern California river plumes (Mertes and Warrick, 2001) and were considerably less than the hypothetical amounts of sediment flux from such events on the rivers (Brownlie and Taylor, 1981). Thus, we suggest that at least 90% of the river suspended-sediment was not observed on the first day of sampling, likely due to high rates of particle settling (cf. Warrick et al., 2004a).

During the subsequent days, both increases and decreases were observed in the sediment:water ratios (Tables 1 and 2), which suggests that both losses and gains of sediment occurred in the sampled plumes. Gains were especially apparent in the Tijuana River system (Table 1).

3.4. Observations of plume transport

Results presented above suggest that plume freshwater was transported significantly beyond the sampled stations. Here we examine measurements of this transport from drifters, HF radar and satellite remote sensing. Ten drifter deployments within plumes revealed many different patterns of plume movement. For example, two contrasting observations from the Santa Ana River plume are shown in Fig. 9. The majority of drifter observations were dominated by alongshore transport, which could exceed 30 cm/s (Fig. 10). Across-shore currents were strongly correlated with alongshore currents but were consistently smaller in magnitude (Fig. 10). Rivers did not appear to influence the across-shore velocity as
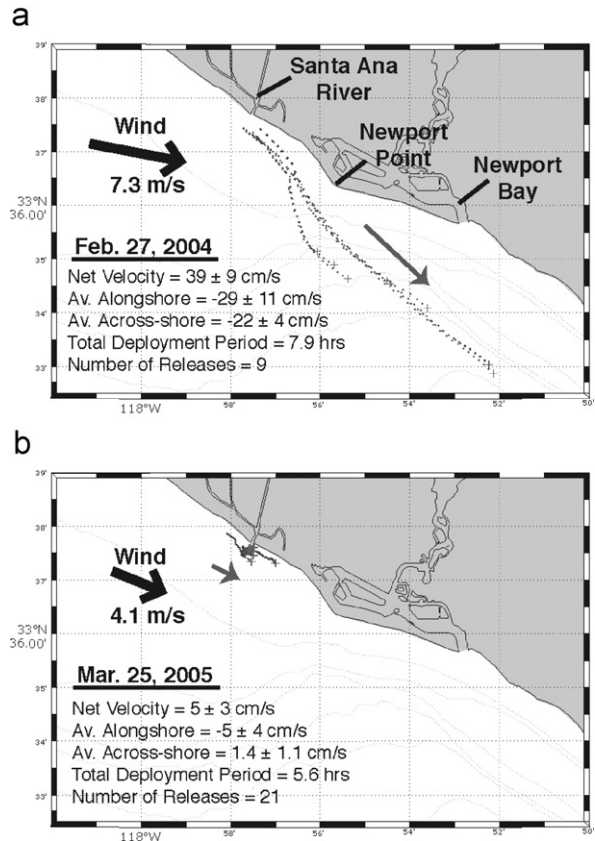

Fig. 9. Drifter results from the Santa Ana River plume during contrasting advection conditions. Positions of each drifter are shown at 10-min increments. Summary statistics for the releases shown in the lower left of each subfigure. Mean wind speed vectors shown for a 6-h period of time prior to the middle of the observations from NDBC 46025.
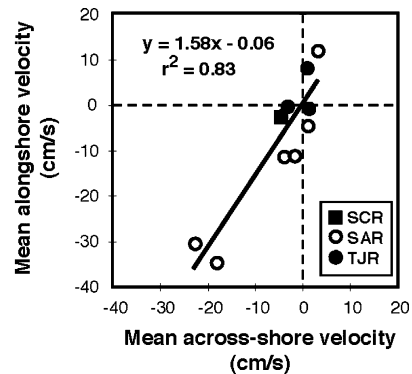

Fig. 10. Mean alongshore and across-shore current velocities from the river plume drifter deployments. Alongshore defined as poleward (positive) and equatorward (negative), and across-shore defined as onshore (positive) and offshore (negative). Rivers plumes monitored include the Santa Clara River (SCR), Santa Ana River (SAR) and Tijuana River (TJR).
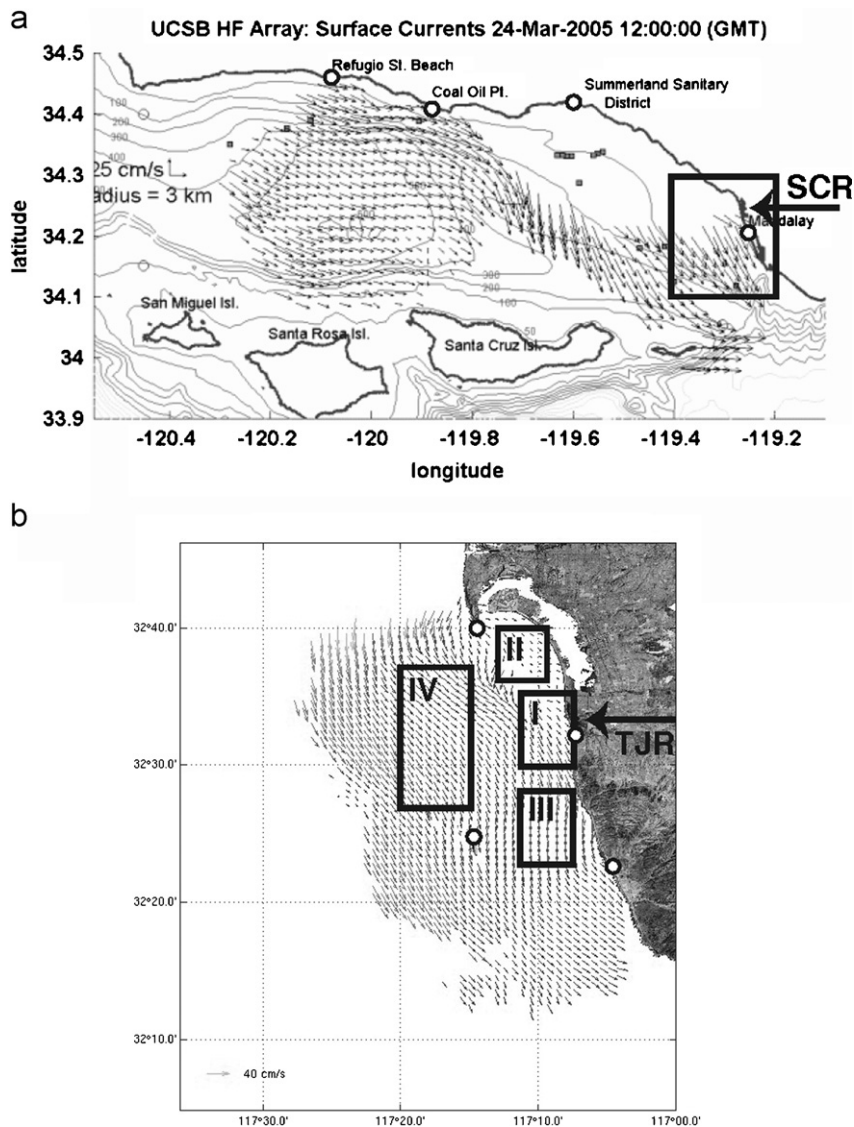
Fig. 11. Example mean daily surface currents from the two HF Radar surface current arrays. Inset boxes show the regions directly offshore of the river mouths for which mean currents were calculated (see text): (a) surface currents near the Santa Clara River mouth (SCR) from the UCSB HF Radar array. (b) Surface currents near the Tijuana River mouth (TJR) from the SIO HF Radar array.

drifter trajectories were not deflected offshore immediately seaward of the river mouths, which was likely related to low river discharge rates on the drifter deployment days (cf. Figs. 2 and 3).

Surface currents were also measured by HF radar arrays in two of the study regions. We spatially subsampled the surface current data into areas relevant to plume movement (Fig. 11). For the Santa Clara River only a region immediately offshore of the river was sampled, while four regions were subsampled for the Tijuana River to evaluate the expected variability of circulation

of this region (cf. Roughan et al., 2005; Fig. 11). The variance of the hourly current measurements within each subsampled region was generally low, and mean hourly standard deviations were 12 cm/s for the Santa Clara, <6 cm/s for all nearshore Tijuana (I–III) and 9 cm/s for offshore Tijuana (IV). For all subregions, we calculated mean daily currents centered on local midnight to best represent total circulation between satellite imagery (obtained approximately at local noon) and to approximate the subtidal portions of the currents.
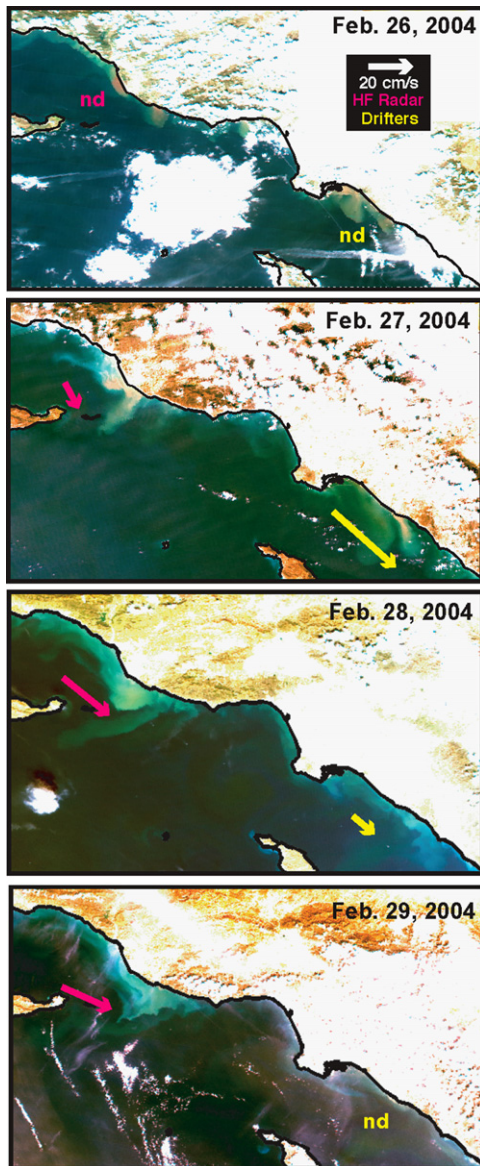
Fig. 12. Four-day time series of true-color satellite imagery from MODIS Aqua and Terra of the northern portion of the study area during the 2004 sampling period. Velocity vectors are shown from the HF Radar observations of the Santa Clara River plume area (pink) and drifter releases offshore of the Santa Ana River (yellow). Days without velocity observations are denoted with "n.d."

Compilations of some of the available HF radar, drifters and satellite imagery are shown in Figs. 12–14. During and following the 2004 event, strong equatorward currents (>30 cm/s) were measured in both the Santa Clara River plume and the San Pedro Shelf regions (Fig. 12). Satellite imagery obtained during this period revealed plume fronts

from the Santa Clara River and San Pedro Shelf regions moving offshore and equatorward at rates (>30 km/d) consistent with the measured current directions (Fig. 12).

During 2005 similar equatorward currents existed and persisted near the Santa Clara River mouth for at least 10 days as shown by HF radar data (Fig. 13). For both events mean currents on the Santa Pedro Shelf were strongest (>30 cm/s) during the first day following river discharge (Figs. 12 and 13). The equatorward currents offshore of the Santa Clara River mouth were clearly responsible for transporting the Santa Clara River plume toward the Santa Monica Bay for a period of at least a week (Fig. 13). During this time long (~50 km) filaments of turbidity, CDOM and perhaps phytoplankton were observed originating near the Santa Clara River and extending into the outside of both Santa Monica and San Pedro Bays (Fig. 13). Both HF radar and satellite data suggest that advection of this plume averaged 15–45 cm/s each day (mean = 26 cm/s), which is fast enough to transport Santa Clara River water into the center of Santa Monica Bay in 2–6 days (mean = 3.5 days).

We note that plumes from Ballona Creek during both events were much more difficult to identify with the satellite imagery than from either the Santa Clara River or San Pedro Bay regions (Figs. 12 and 13), which may be due to the small size and/or quick dispersal of this plume.

Satellite and HF radar observations for the Tijuana River plume show that circulation in the Tijuana River plume region was complex during the events (Fig. 14). A counterclockwise eddy was observed south of Pt. Loma during February 23–26, 2004, which changed to southerly flow conditions on February 27–29, 2004. We note that the mean daily alongshore currents furthest offshore of the Tijuana River (region IV, Fig. 11b) explained 60%, 51% and 76% of the alongshore mean current variance in three inshore regions (I—river mouth, II—north of mouth, III—south of mouth), respectively during the 2004 and 2005 events. Thus, although there is spatial variability in the currents, there was relatively strong coherence in the current patterns during the events sampled.

3.5. Transport forcing

In this section, we examined a number of plume transport forcing parameters to evaluate why the
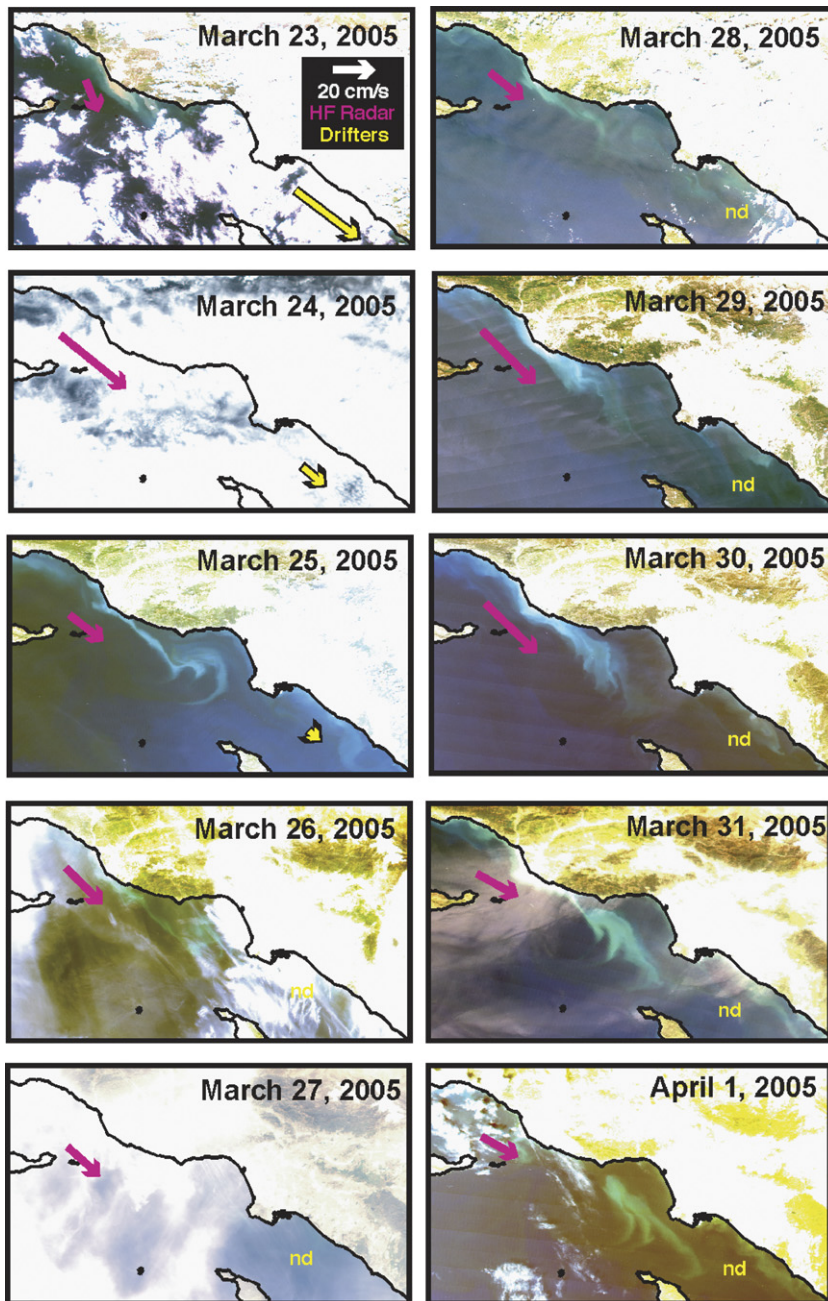
Fig. 13. Ten-day time series of true-color satellite imagery from MODIS Aqua and Terra of the northern portion of the study area during the 2005 sampling period. Velocity vectors are also shown from the HF Radar observations of the Santa Clara River plume area (pink) and drifter releases offshore of the Santa Ana River (yellow). Days without velocity observations are denoted with "n.d."

plumes transported in the manner they did. Our techniques closely follow those of Garvine (1995), Geyer et al. (2000), Fong and Geyer (2002), and Whitney and Garvine (2005). A synthesis of these results is included in the Discussion section.

First, the baroclinic height anomaly (h_f) was calculated assuming hydrostatic pressure with the baroclinic pressure anomaly (P_f), such that,

$$h_f = P_f/g\rho_0, \tag{3a}$$

where

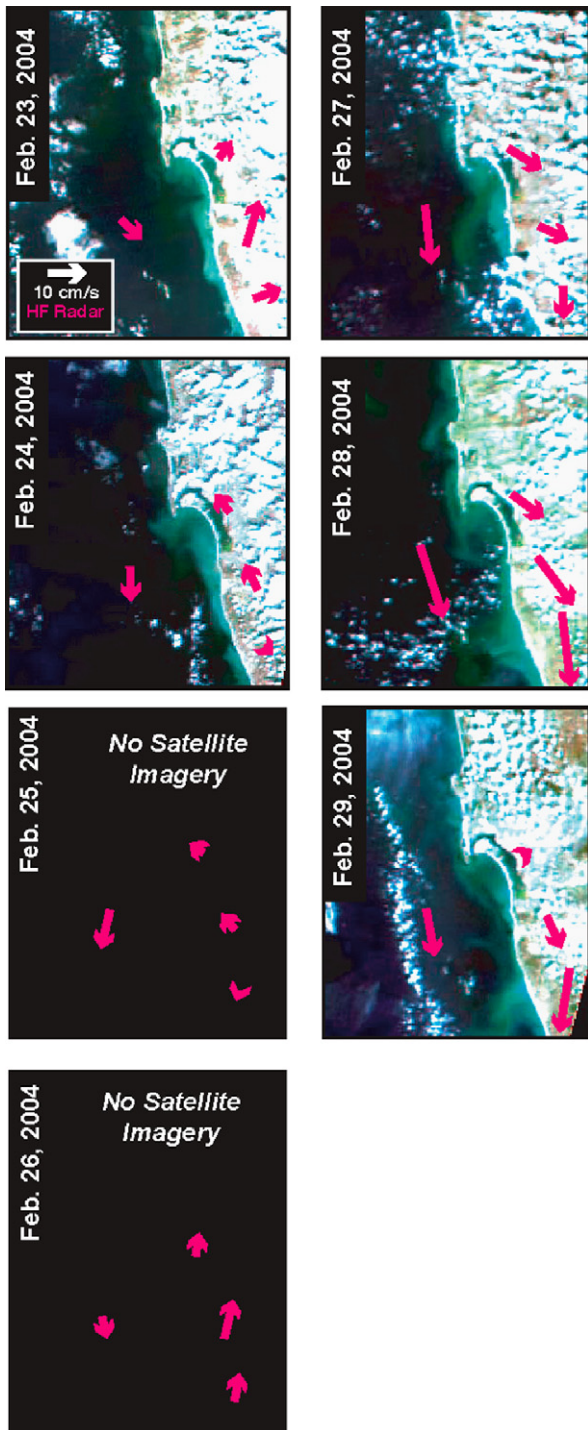$$P_f = g \int_h [\rho_0 - \rho(z)]\,dz \tag{3b}$$

Fig. 14. True-color satellite imagery from MODIS Aqua and Terra of the southern portion of the study area during the 2004 sampling period. Mean daily velocity vectors are also shown from the HF radar observations of the Tijuana River plume area (pink). Vectors have been placed on land immediately adjacent to the sampled regions so that the coastal plumes are not obscured.

and g is the gravitational constant, ρ_0 is the ambient seawater density, $\rho(z)$ is the density at depth z, and h is the total water depth. The maximum h_f for each cruise was consistently measured on the first day of sampling and ranged between 0.0 and 1.7 cm across the sites (Table 3). Values of h_f were consistently lower for the Santa Clara River plume than for the remaining sites.

Secondly, the baroclinic velocity anomaly (u_f) provides an estimate for the initial plume velocity associated with buoyancy forcing at the river mouth and was computed using Bernoulli's equation and h_f,

$$u_f = (2gh_f)^{0.5}. \tag{4}$$

The maximum values of this baroclinic velocity were generally 20–55 cm/s during each cruise (Table 3).

If the plumes resulted in geostrophic momentum balances, Fong and Geyer (2002) suggest that the alongshore velocity of this transport can be approximated by

$$v = g'h_0/fL \tag{5}$$

where g' is the reduced gravitational constant resulting from the plume (equivalent to $g\,\Delta\rho/\rho_0$), h_0 is the thickness of the plume nearest the coast, f is the Coriolis parameter ($\sim 8.2 \times 10^{-5}$/s) and L is the plume width offshore of the coastline. Using maximum values for g' and h_0 for each cruise and assuming L was O(10) km, geostophic velocities were computed to be O(10) cm/s (Table 3). We note that these velocities would be directed poleward, which is both smaller and in the opposite direction of the majority of observations presented here (Figs. 12–14).

We next looked into the effects of winds on the buoyant river following a number of previous studies (e.g., Chao 1988; Munchow and Garvine, 1993; Kourafalou et al., 1996; Geyer et al., 2000; Whitney and Garvine, 2005). We examined both wind speed and wind stress, and wind speed provided the best correlations with plume velocity observations, consistent with the theory and observations presented by Garvine (1991) and Whitney and Garvine (2005). Mean alongshore currents measured by the drifters were significantly correlated to local alongshore wind speed ($r^2 = 0.66$, $p < 0.01$; Fig. 15). Maximum correlation was found for the mean winds occurring during the 6-h prior to the middle of the drifter release periods.

Table 3
Plume forcing statistics from the CTD+ casts during 2004 and 2005

|	Santa Clara River	Ballona Creek	San Pedro Shelf	San Diego River	Tijuana River
Maximum salinity anomaly (cm)					
2004 cruise	1	26	58	5	7
2005 cruise	7	27	32	n.d.	14
Maximum baroclinic height anomaly (cm)					
2004 cruise	0.01	0.73	1.67	0.25	0.27
2005 cruise	0.18	1.16	1.22	n.d.	1.57
Maximum baroclinic velocity anomaly (cm/s)					
2004 cruise	4.8	37.9	57.3	21.9	23.1
2005 cruise	18.6	47.6	48.8	n.d.	55.5
Geostrophic Velocity (cm/s)					
2004 cruise	0.1	5.7	13.1	1.9	2.1
2005 cruise	1.4	9.0	9.5	n.d.	12.3
Wind stress index ($|Ws|$)					
Peak discharge	0.3–0.8	0.4–0.6	0.4–0.5	0.4–0.6	0.4–0.6
Peak wind	1.8	>2	1.5	1.6	1.6
Linear slope of wind–current correlation					
Mean	0.039	n.d.	0.033	n.d.	0.027
95% confidence interval	0.013	n.d.	0.016	n.d.	0.006
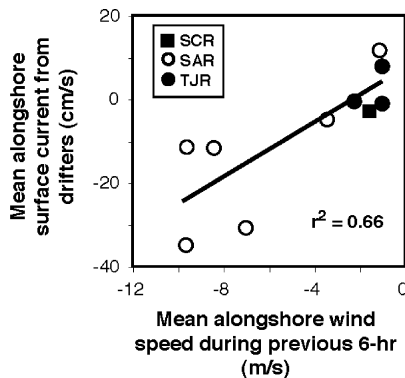
Fig. 15. The relation between alongshore wind speed and mean alongshore surface currents measured for drifters. Maximum correlation occurs for the mean wind stress during the 6-h prior to the deployment. Alongshore defined as poleward (positive) and equatorward (negative). River plumes monitored include the Santa Clara River (SCR), Santa Ana River (SAR) and Tijuana River (TJR).

Stronger correlations were found between mean daily wind speed and mean daily plume velocity immediately offshore of the river mouths from the HF radar data (Fig. 16). High correlations were found at zero lag for 24-h averages ($r^2 = 0.68$–0.71), but peak correlations occurred for mean 24-h winds that were lagged by 3 h compared to currents ($r^2 = 0.71$–0.74; Fig. 16). This observation is consistent with a multiple hour lag for maximum

correlation in wind-plume response by Munchow and Garvine (1993) and Geyer et al. (2000). For the regions immediately offshore of the Santa Clara and Tijuana river mouths, mean daily wind speed explained 71–74% of the alongshore surface current variance and captures most of the temporal shifts in these currents (Fig. 16). Across-shore surface currents were somewhat poorly correlated with wind speed (maximum $r^2 = 0.28$–0.44, data not shown).

Further evaluation of the influence of wind can be provided by a framework suggested by Whitney and Garvine (2005). They propose that the wind stress index (W_s) can determine whether a plume's along-shelf flow is wind- or buoyancy-driven, where W_s is the ratio of buoyancy-driven velocity (u_{dis}) and the wind-driven alongshore velocity (u_{wind}). The first variable can be evaluated by either considering a two-layer system in geostrophic balance, which may be reduced to

$$u_{dis} = K^{-1}(2g'_r Qf)^{1/4}, \qquad (6)$$

where K is the dimensionless current width (or Kelvin number), which is ~1 for southern California plumes (Warrick et al., 2004b), g'_r is the reduced gravity of the river water (~0.24 m/s^2 assuming 32 psu ambient seawater and 0 psu river water both at 10 °C), Q is the volumetric river discharge rate, and f is the Coriolis parameter, or by using Eq. (4) to solve for u_f if the plume is not geostrophic.
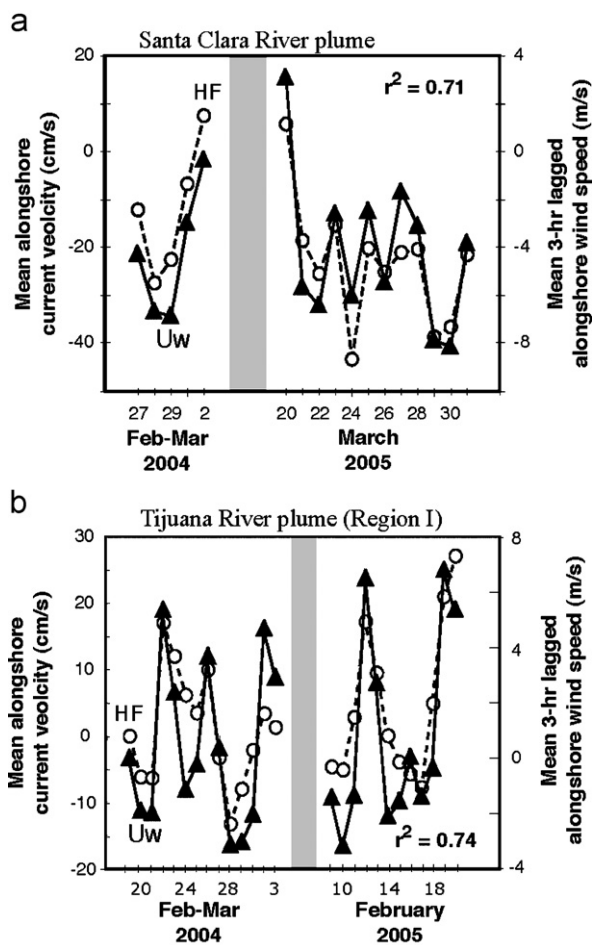
Fig. 16. The relation between mean daily alongshore wind speed (▲) and mean daily surface currents of river plumes from HF radar (○) during sampled events: (a) Santa Clara River plume with 24-h mean wind speed from the NDBC East Santa Barbara Channel buoy (46053) lagged by a 3-h preceding period. (b) Tijuana River plume (region I in Fig. 15b) with 24-h mean wind speed from the NDBC San Clemente Basin buoy (46086) lagged by 3-h. Correlation coefficients given for the linear regression between currents and winds. Alongshore defined as poleward (positive) and equatorward (negative).

Assuming a barotropic wind response, a steady-state momentum balance between wind stress and bottom stress, and quadratic drag laws, Whitney and Garvine (2005) suggest that u_{wind} can be estimated by

$$u_{wind} = \{(\rho_{air}/\rho)(C_{10}/C_{Da})\}^{1/2}U \qquad (7)$$

where ρ_{air} and ρ are the density of air and seawater, C_{10} and C_{Da} are the drag coefficients for the air–sea boundary and the seabed, and U is the alongshore component of the wind speed. It can be shown that u_{wind} is equal to $\sim 0.0265U$ under the assumptions given above (Whitney and Garvine, 2005). When the

absolute value of W_s is less than one, a river-induced buoyancy current should dominate. However when W_s is greater than one, the plume should be dominated by wind-driven flow. Upwelling-favorable winds will arrest or, perhaps, reverse a buoyant geostrophic coastal current, whereas down-welling-favorable winds will enhance the current.

Using this framework, we computed W_s for the time series of daily mean discharge and wind records surround the sampled events. On peak days of river discharge $|W_s|$ ranged between 0.3 and 0.8 (Table 3). Peak winds often occurred within 1–3 days after the peak discharge, during which $|W_s|$ ranged from 1.5 to over 2, suggesting wind-driven flow (Whitney and Garvine, 2005). If the assumptions made above hold, then the linear slope between U and u_{wind} should be approximately 0.0265. Using data presented in Figs. 15 and 16, we computed linear slopes between winds and currents that were somewhat higher but statistically indistinguishable from this theoretical value (Table 3).

Finally, we computed the wind strain timescale (t_{tilt}), which is defined by the time is takes for Ekman transport to either compress a plume toward the shoreline during downwelling winds or expand a plume offshore by upwelling winds by a scale of 2 (Whitney and Garvine, 2005), and can be approximated by

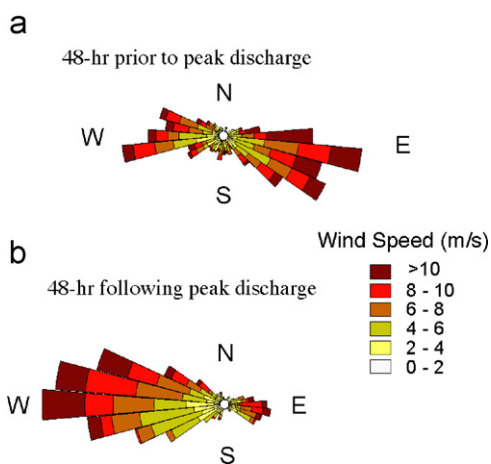$$t_{tilt} = (KRh_1\rho f)/(16|\tau_{sx}|), \qquad (8)$$

Fig. 17. Wind rosettes from the East Santa Barbara Channel (NDBC 46053) during the 48-h prior to and following peak discharge in the Santa Clara River from 15-min discharge data. Wind is oriented to the direction from which the wind originated and was compiled for the 18 events in excess of 25 m³/s during the period overlapping records (1994–2004).

where K is approximately 1 (Warrick et al., 2004b), the internal Rossby radius (R) is approximately 10^4, the plume thickness (h_1) is ~3 m, ρ is ~1024 kg/m^3, and the alongshore wind stress (τ_{sx}) is calculated with the quadratic drag laws described above. Using Eq. (8), t_{tilt} values for wind speeds of 2, 4 and 8 m/s were computed to be 8, 2 and 0.5 h, respectively. Thus, for the wind speeds typically observed during and immediately following river discharge events (cf. Figs. 16 and 17), the effect of wind occurs on time-scales much shorter than a day.

4. Discussion

Previous studies have established, primarily through the use of satellite imagery, that southern California river plumes are transported 10's of km offshore. Our study indicates that alongshore movement of these plumes can be more prevalent than across-shore movement. Mean daily alongshore plume advection, as measured by drifters, HF radar and satellite was as high as 50 cm/s, suggesting that contaminants discharged from a river system can be quickly transported to coastal waters offshore of adjacent basins. This was especially apparent for the Santa Clara River plume, which was observed to extend toward Santa Monica Bay during all of our observations.

The plumes were also found to retain their integrity as they advected along the coast. While the salinity signature of the river discharge changed dramatically within the first kilometer of mixing with ocean water (i.e., inshore of our ship measurements), the plumes were clearly distinguishable as a water mass for at least 5 days following a storm. This distinction was apparent in both lateral and vertical dimensions, extending 10's of km and several meters, respectively. Unfortunately we could not calculate rates of vertical mixing with the CTD+ data, largely because of the strong lateral movements that prevented resampling of water masses.

Although there is widespread consensus that local wind stress explains little of the current variability within the Southern California Bight (e.g., Lentz and Winant, 1986; Noble et al., 2002; Hickey et al., 2003), we found that wind was an important, and often the dominant, forcing function for transport of the river plumes. We note that although wind explained only 66% of the alongshore current variability as measured by the drifters, we did not attempt to remove tidal effects from these data, which would likely improve correlations.

Because winter storms are related to broad atmospheric low-pressure systems moving across southern California, wind patterns are commonly poleward (downwelling) prior to river discharge and equatorward (upwelling) following discharge (Winant and Dorman, 1997; Nezlin and Stein, 2005). An example of this can be seen in the winds of the Santa Barbara Channel during the 48-h before and after river discharge events (Fig. 17). During the 48-h following a discharge event, winds are four times more likely to be upwelling (from the west) than downwelling, and ~80% of these winds are greater than 4 m/s. Post-storm variability in wind stress will be related to broad atmospheric conditions across the eastern Pacific and western North America. The 11-day period of upwelling winds following the March 2005 event (Fig. 16a) was related to a transition to spring conditions of upwelling-dominated wind and appears to be uncommonly long. Post-storm upwelling winds appear to more commonly last only 1–5 days following an event.

We note here that wind explained more of the surface current variance immediately offshore of the Tijuana River mouth than for any of the adjacent coastal subregions measured with HF radar (Fig. 18). Hydrographic surveys of this broad region show that freshwater-induced stratification was consistently strongest immediately offshore of the river during the time considered. These combined results are consistent with observations that shallow stratification increases the response of surface currents to wind stress (e.g., Chao, 1988; Kourafalou et al., 1996). The poor-relationship
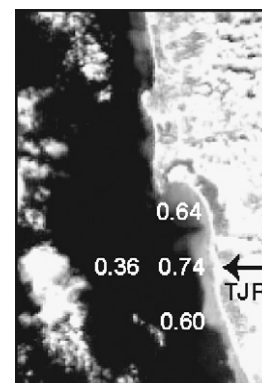

Fig. 18. Maximum correlation coefficient (r^2) for linear regression between lagged mean daily alongshore wind speed at NDBC 46086 and mean daily alongshore HF radar surface currents within the four regions identified in Fig. 11b.

($r^2 = 0.36$) in the offshore region was consistent both with lower measured levels of stratification in this region and with the observation by Lentz and Winant (1986) that wind stress becomes less important in the momentum balance with depth on the southern California shelf.

Thus, winds explained a majority of the plume transport variance over temporal scales of days. Due to the temporal coherence of winds and river discharge (e.g., Fig. 17), river plumes are commonly observed to flow to the left after leaving the river mouths, which is opposite of the expected direction due to Coriolis (Yankosky and Chapman, 1997). Although wind-dominance is observed in a number of river plume systems throughout the world (e.g., Hickey et al., 2005; Whitney and Garvine, 2005; Piñones et al., 2005), we note that the southern California plumes are distinctive in that the discharge events occur over time scales of hours and the winds are temporally coherent with discharge and have time scales of days. Thus, the upwelling wind-dominance of southern California river plumes is a common condition. Other river plumes have much longer discharge events, which may or may not be coherent with winds, resulting in less regular wind-dominance or alternating direction of wind-dominance (Hickey et al., 2005; Whitney and Garvine, 2005; Piñones et al., 2005).

We fully expect that other factors, such as river discharge inertia, buoyancy-related currents, tidal currents, and non-wind generated subtidal currents, also have significant effects on plume advection within specific scales of space and time. For example, tidal currents were observed in the hourly HF radar data with magnitudes of 5–15 cm/s, and although these currents are important to instantaneous plume advection, they generally induced no net current over daily time scales. Further, we computed values of plume-induced baroclinic velocities of up to 20–55 cm/s (Table 3), which suggests that initial advection of the plumes at the river mouths was quite rapid in response to this buoyancy. The initial advection was also likely influenced by river discharge inertia from the velocity of the river flux ($\sim$50 cm/s; cf. Warrick et al., 2004b). The jet-like plume shapes observed by satellite on February 26, 2004 (Fig. 12) likely result from these high initial velocities (cf. Garvine, 1995). We calculate that the four visible plume fronts in this image advected $\sim$20 km from the river mouths, which is equivalent to a mean velocity of $\sim$45 cm/s since the peak discharge in the rivers (cf. Fig. 2). We

note that these initial (i.e., 12-h) velocities appear to be strongly across-shore in direction, which differs from the alongshore-dominated transport measured later during the events. Lastly, geostrophic velocities were computed to be small compared to actual observed velocities and also directed in the opposite direction of the majority of observations. Thus, we suggest that geostrophic flows were generally much weaker than wind-induced flows, which is consistent with calculations of W_s and t_{tilt} above and Santa Monica Bay observations of Washburn et al. (2003). Summarizing, plume advection appears to be dominated by river discharge inertia and buoyancy within a few hours and kilometers of the river mouth, while winds dominate plume advection during the subsequent days.

Accurately describing these storm-induced river plumes required a combination of assessment tools. Ships provided the best information, but the rapidity of plume evolution outpaced ship movement while sampling. Even with the large number of ships that were mustered for this study, we found that almost half of the plume water volume occurred outside of the area able to be sampled within the first study day. In addition we found that ships were unable to sample on several of the days most critical to plume evolution, as the high winds that typically follow a storm event led to an unsafe sea state (cf. Nezlin et al., 2007).

Satellites provided a valuable synoptic view, but once or twice per day (at best) frequency of the moderate-resolution polar orbiting satellites is temporally insufficient to describe the rapidly evolving plume. Moreover, these images are often obscured by cloud cover (Nezlin et al., 2007), further reducing their temporal resolution. High frequency radar provided a continuous synoptic view but only provided surface currents, without definition of plume edge. Drifters provided a Lagrangian perspective of surface currents that could be utilized real-time to track plume advection or in retrospective analyses of current forcing. Although not utilized here, we suggest that autonomous underwater vehicles (AUVs) would fill important information gaps on the movement and mixing of water properties when ships are not able to sail and cloud-cover prevents satellite observations. When combined altogether we found that these techniques provided essential information to track plumes and better understand the transport of watershed-derived pollutants and pathogens in the coastal ocean.

Future identification of discharged river water and its water quality impacts throughout the Southern California Bight will require tracers of the discharged water and pollutants. Although salinity is surely the best plume tracer, it can only be readily measured *in situ* with conductivity/temperature sensors, which limits the timing and locations of observations. Measurements of salinity from remote platforms have great potential and would provide a valuable synoptic overview, but these observations are presently limited to an experimental basis using airborne sensors. Further, it is not clear how well these emerging capabilities will be able to adequately resolve and characterize the small-scale variability and narrow ranges of salinity often observed in these coastal regions. Our results suggest that the optical properties of CDOM may be effectively exploited to track plumes in southern California and could serve as better tracers than suspended sediment or turbidity observations. This is especially relevant for future identification and tracking of plumes with remotely sensed imagery (e.g., Mertes and Warrick, 2001; Nezlin et al., 2005), and we suggest further investigation of the use of CDOM absorption and other satellite ocean-color-derived products to monitor the distribution of plumes and assess their ecological impacts.

5. Conclusions

The combined use of ship-based sampling and remotely sensed ocean imagery provided new insights into the patterns and dynamics of river plumes offshore of the largest southern California watersheds. Plumes were observed to quickly move from the river mouths and to respond strongly and quickly to winds. The combined measurements clearly show how plume waters were transported to adjacent portions of the Southern California Bight within days of discharge. This suggests that water quality and ecological impacts from outflow of a watershed may be exhibited in portions of the coastal ocean far from this source watershed. Considering that these plumes are important vectors for land-based pollutants, pathogens and nutrients, better understanding is needed of the water quality and ecological implications and impacts of these plumes.

Acknowledgements

References

Ahn, J.H., Grant, S.B., Surbeck, C.Q., DiGiacomo, P.M., Nezlin, N.N., Jiang, S., 2005. Coastal water quality impact of storm water runoff from an urban watershed in southern California. Environmental Science and Technology 39, 5940–5953.

Baker, E.T., Lavelle, J.W., 1984. The effect of particle size on the light attenuation coefficient of natural suspensions. Journal of Geophysical Research 89, 8197–8203.

Brownlie, W.R., Taylor, B.D., 1981. Sediment management for Southern California mountains, coastal plains and shoreline; part C, coastal sediment delivery by major rivers in Southern California. Environmental Quality Laboratory Report No. 17-C, California Institute of Technology. Pasadena, CA.

Chao, S.Y., 1988. Wind-driven motion of estuarine plumes. Journal of Physical Oceanography 18, 1144–1166.

DiGiacomo, P.M., Washburn, L., Holt, B., Jones, B.H., 2004. Coastal pollution hazards in southern California observed by

SAR imagery: stormwater plumes, wastewater plumes, and natural hydrocarbon seeps. Marine Pollution Bulletin 49, 1013–1024.

Dojiri, M., Yamaguchi, M., Weisberg, S.B., Lee, H.J., 2003. Changing anthropogenic influence on the Santa Monica Bay watershed. Marine Environmental Research 56, 1–14.

Fong, D.A., Geyer, W.R., 2002. The alongshore transport of freshwater in a surface-trapped river plume. Journal of Physical Oceanography 32, 957–972.

Garvine, R.W., 1991. Subtidal frequency estuary-shelf interaction: observations near Delaware Bay. Journal of Geophysical Research 96, 7049–7064.

Garvine, R.W., 1995. A dynamical system for classifying buoyant coastal discharges. Continental Shelf Research 15 (3), 1585–1596.

Geyer, W.R., Hill, P., Milligan, T., Traykovski, P., 2000. The structure of the Eel River plume during floods. Continental Shelf Research 20, 2067–2093.

Gilbert, P.S., Lee, T.N., Podesta, G.P., 1996. Transport of anomalous low-salinity waters from the Mississippi River flood of 1993 to the Straits of Florida. Continental Shelf Research 16 (8), 1065–1085.

Hickey, B.M., Dobbins, E.L., Allen, S.E., 2003. Local and remote forcing of currents and temperature in the central Southern California Bight. Journal of Geophysical Research 108, 1–26.

Hickey, B.M., Geier, S., Kachel, N., MacFadyen, A., 2005. A bi-directional river plume: the Columbia in summer. Continental Shelf Research 25, 1631–1656.

Inman, D.L., Jenkins, S.A., 1999. Climate change and the episodicity of sediment flux of small California rivers. Journal of Geology 107, 251–270.

Jones, B.H., Washburn, L., 1997. Stormwater runoff into Santa Monica Bay: identification, impact and dispersion. In: Magoon, O.T., Converse, H., Baird, B., Miller-Henson, M. (Eds.), California and the World Ocean '97. American Society of Civil Engineers, Reston, VA.

Kourafalou, V.H., Lee, T.N., Oey, L.Y., Wang, J.D., 1996. The fate of river discharge on the continental shelf 2. Transport of coastal low-salinity waters under realistic wind and tidal forcing. Journal of Geophysical Research 101, 3435–3455.

Large, W.G., Pond, S., 1981. Open ocean momentum flux measurements in moderate to strong winds. Journal of Physical Oceanography 11, 324–336.

Lentz, S.J., Winant, C.D., 1986. Subinertial currents on the southern California shelf. Journal of Physical Oceanography 16, 1737–1750.

Mertes, L.A.K., Warrick, J.A., 2001. Measuring flood output from 110 coastal watersheds in California with field measurements and SeaWiFS. Geology 29, 659–662.

Munchow, A., Garvine, R.W., 1993. Buoyancy and wind forcing of a coastal current. Journal of Marine Research 51, 293–322.

Nezlin, N.P., DiGiacomo, P.M., 2005. Satellite ocean color observations of stormwater runoff plumes along the San Pedro Shelf (Southern California) during 1997–2003. Continental Shelf Research 25, 1692–1711.

Nezlin, N.P., DiGiacomo, P.M., Stein, E.D., Ackerman, D., 2005. Stormwater runoff plumes observed by SeaWiFS radiometer in the Southern California Bight. Remote Sensing of Environment 98, 494–510.

Nezlin, N.P., Stein, E.D., 2005. Spatial and temporal patterns of remotely-sensed and field measured rainfall in southern California. Remote Sensing of Environment 96 (2), 228–245.

Nezlin, N.P., Warrick, J.A., DiGiacomo, P.M., Jones, B., Schnetzer, A., in preparation. MODIS imagery as a tool for water quality assessments in the southern California coastal ocean. SPIE 2007 Optics and Photic Conference Proceedings, International Society for Optical Engineering, Bellingham, WA, submitted for publication.

Nezlin, N.P., Weisberg, S.B., Diehl, D.W., 2007. Relative availability of satellite imagery and ship sampling for assessment of stormwater runoff plumes in coastal southern California. Estuarine, Coastal and Shelf Science 71 (1–2), 250–258.

Noble, M.A., Ryan, H.F., Wiberg, P.L., 2002. The dynamics of subtidal poleward flows over a narrow continental shelf, Palos Verde, CA. Continental Shelf Research 22, 923–944.

Ohlmann, J.C., 2005. A new kind of drifter to observe the coastal ocean. Bulletin of the American Meteorological Society 86, 1219–1220.

Piñones, A., et al., 2005. Wind-induced diurnal variability in river plume motion. Estuarine, Coastal and Shelf Science 65, 513–525.

Roughan, M., Terrill, E.J., Largier, J.L., Otero, M.P., 2005. Observations of divergence and upwelling around Point Loma, California. Journal of Geophysical Research 110, C04011.

Schiff, K., Bay, S., Allen, M.J., Zeng, E., 2001. Southern California. Marine Pollution Bulletin 41, 76–93.

Southern California Water Research Project (SCCWRP), in preparation. Southern California Bight 2003 Regional Monitoring Program: IV. Water Quality. Southern California Water Research Project, Costa Mesa, California.

Stein, E.D., Tiefenthaler, L.L., Schiff, K.C., 2006. Watershed-based sources of polycyclic aromatic hydrocarbons in urban storm water. Environmental Toxicology and Chemistry 25, 373–385.

Stumpf, R.P., Gelfenbaum, G., Pennock, J.R., 1993. Wind and tidal forcing of a buoyant plume, Mobile Bay, Alabama. Continental Shelf Research 13 (11), 1281–1301.

Warrick, J.A., Milliman, J.D., 2003. Hyperpycnal sediment discharge from semiarid southern California rivers: implications for coastal sediment budgets. Geology 31, 781–784.

Warrick, J.A., Fong, D.A., 2004. Dispersal scaling from the world's rivers. Geophysical Research Letters 31, L04301.

Warrick, J.A., Mertes, L.A.K., Washburn, L., Siegel, D.A., 2004a. A conceptual model for river water and sediment dispersal in the Santa Barbara Channel, California. Continental Shelf Research 24, 2029–2043.

Warrick, J.A., Mertes, L.A.K., Siegel, D.A., Washburn, L., 2004b. Dispersal forcing of a southern California river plume, based on field and remote sensing observations. Geo-Marine Letters 24, 46–52.

Warrick, J.A., Washburn, L., Brzezinski, M.A., Siegel, D.A., 2005. Nutrient contributions to the Santa Barbara Channel, California, from the ephemeral Santa Clara River. Estuarine, Coastal and Shelf Science 62, 559–574.

Washburn, L., McClure, K.A., Jones, B., Bay, S.M., 2003. Spatial scales and evolution of stormwater plumes in Santa Monica Bay. Marine Environmental Research 56, 103–125.

Whitney, M.M., Garvine, R.W., 2005. Wind influence on a coastal buoyant outflow. Journal of Geophysical Research 110, C3014.

Willis, C.M., Griggs, G.B., 2003. Reductions in fluvial sediment discharge by coastal dams in California and implications for beach sustainability. Journal of Geology 111, 167–182.

Winant, C.D., Dorman, C.E., 1997. Seasonal patterns of surface wind stress and heat flux over the Southern California Bight. Journal of Geophysical Research 102, 5641–5654.

Yankosky, A.E., Chapman, D.C., 1997. A simple theory for the fate of buoyant coastal discharges. Journal of Physical Oceanography 27 (7), 1386–1401.